Stimulated emission of a microcavity dressed exciton and suppression of phonon scattering

Stanley Pau, Gunnar Björk, Joseph Jacobson, Hui Cao, and Yoshihisa Yamamoto*
Exploratory Research for Advanced Technology Quantum Fluctuation Project, Edward L. Ginzton Laboratory, Stanford University, Stanford, California 94305
(Received 16 September 1994; revised manuscript received 15 November 1994)

The threshold behavior of the stimulated parametric emission of dressed excitons in a microcavity is studied. The inelastic-phonon-scattering rates of the dressed exciton are calculated and are shown to be smaller than the bare quantum-well exciton values. The results describe the recently observed thresholdless photoemission behavior and predict a large stability for the dressed exciton modes inside a quantum-well microcavity.

I. INTRODUCTION

Recent observations of thresholdless coherent spontaneous emission with $\beta = 1$,[1] normal mode (vacuum Rabi) splitting,[2] and picosecond oscillating emission[3] in quantum-well microcavities at low temperature open up the possibility of very low power and fast excitonic light emitting devices. The behavior of the exciton resonantly coupled to the microcavity photon mode can be modeled as coupled harmonic oscillators between which the energy is cycling back and forth. It is well known that such a system does not exhibit a nonlinear threshold.[4–6] In this paper, we study the emergence of a threshold for the dressed exciton system inside the microcavity as a function of temperature. The equations of motion for the microcavity polaritons are derived in the Heisenberg picture using the exciton-photon-phonon Hamiltonian and are shown to have the form of the driven-damped harmonic oscillator,[7] in which the coupling constant is dependent on the phonon population. This is different from the atom-photon coupling in a conventional semiconductor laser, where the lasing threshold occurs when the average number of lasing photon is unity.[8] We believe that the dressed exciton picture is the correct one to use because we observe normal mode splitting and reversible oscillatory emission.[3] We define the dressed exciton and polariton modes as the coupled mode of the two-dimensional (2D) exciton and the microcavity photon mode. In a high Q microcavity, the 2D exciton with wave vector $k_{\|} = 0$ can couple to a single planar microcavity photon mode which is spatially stationary, leading to a temporally quasistationary normal mode, the microcavity dressed exciton. The 2D excitons with $k_{\|} \neq 0$ also couple to a continuum of microcavity photon modes which have net propagation along the quantum-well plane, leading to a propagating microcavity polariton. The term dressed exciton is used for the $k_{\|} = 0$ polariton in analogy to the dressed atom in atomic cavity quantum electrodynamic. We use this nomenclature for the spatially stationary polariton because the polariton concept is often associated with propagating waves and the $k_{\|} = 0$ polariton does not propagate. In Sec. II, we present the microcavity polariton dispersion for the heavy hole $1s$ exciton level coupling to a one dimensional continuum of photon modes. In Sec. III, the inelastic scattering rates between the dressed exciton and the polariton via phonon scattering in a GaAs quantum well are calculated as function of temperature and exciton-photon coupling. In Sec. IV, we derive a rate equation of the dressed exciton-polariton dynamics from the polariton Hamiltonian using adiabatic and Markoff approximations. We then solve the equation both numerically and analytically. The theoretical results are compared with recent experiment. In the final section, we discuss the limitations of our model and give a brief summary of our results.

II. MICROCAVITY DRESSED EXCITON AND POLARITON

For a review of the polariton concept, the reader is referred to a recent paper by Andreani.[9] The geometry of the system is depicted in Fig. 1. The exciton is confined to two dimensions inside the quantum well, and we consider only the lowest $1s$ heavy hole exciton with dispersion,

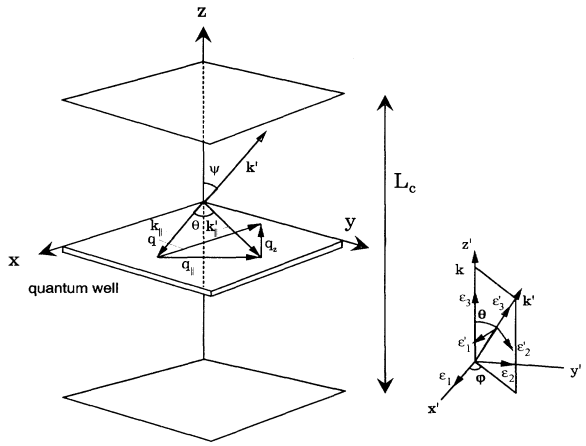

FIG. 1. Structure of quantum-well inside a microcavity. The polarization vectors of the initial and final scattered polariton states are also shown.

$$E_{\rm ex}(k_{\|}) = E_{1s} + \frac{\hbar^2 k_{\|}^2}{2M}, \tag{1}$$

where E_{1s} is the energy of exciton including the lowest order quantization energy, M is the exciton effective mass, and $k_{\|}$ is the wave vector parallel to the plane of the quantum well. For the photon inside the microcavity, we consider the lowest order longitudinal mode where the dispersion is

$$E_p(k_{\|}) = \frac{\hbar c}{n}\sqrt{k_{\|}^2 + \frac{\pi^2}{L_c^2}} = \sqrt{\left(\frac{\hbar c k_{\|}}{n}\right)^2 + E_{1s}^2}, \tag{2}$$

with c being the speed of light in vacuum, n being the refractive index, L_c being the effective cavity length, and we choose $E_p(0) = E_{\rm ex}(0)$ so that the microcavity resonance coincides with the exciton resonance at $k_{\|} = 0$. In addition, we treat the phonon field as a three dimensional bath so that we can neglect surface phonon mode and phonon quantum-well effects.[10] We consider both the optical and acoustic phonon modes and treat the exciton as two dimensional so that only a single exciton subband is considered. For the phonon modes, we take the simple dispersions $E_a(q) = \hbar u\,|q|$, where u is the sound velocity in the semiconductor, and $E_a(q) = \hbar\omega_a$ for the acoustic and optical modes, respectively. We note that in using the above dispersion for the acoustic mode, we must use the Debye cutoff frequency, $\omega_D^3 = 6\pi^2 u^3 N/V$, where N/V is the number of primitive cell per volume, when summing over all the phonon states. The Hamiltonian of the coupled exciton-photon-phonon system, to first order in coupling, is given by[11,12]

$$H = \sum_k \Bigg\{ E_p(k)(a_k^\dagger a_k + \tfrac{1}{2}) + E_{\rm ex}(k)(b_k^\dagger b_k + \tfrac{1}{2}) + E_a(k)(c_k^\dagger c_k + \tfrac{1}{2}) + iE_{1s}\sqrt{\frac{\pi\beta E_{\rm ex}(k)}{\epsilon_\infty E_p(k)}}(a_k^\dagger + a_{-k})(b_k - b_{-k}^\dagger)$$
$$+ \frac{\pi\beta E_{1s}^2}{\epsilon_\infty E_p(k)}(a_k^\dagger + a_{-k})(a_k + a_{-k}^\dagger)\Bigg\} + \sum_{k,k',q} iC(k,k',q) b_{k'}^\dagger b_k (c_q - c_{-q}^\dagger)\delta(k' - k - q), \tag{3}$$

where a_k, b_k, and c_k are the annihilation operators of the microcavity photon, the quantum-well exciton, and the phonon, respectively, and we neglect any direct coupling between phonon and photon. We also assume that the phase space filling effect is negligible so that the exciton is bosonic. The phonon-exciton coupling constant $C(k,k',q)$ is that for the three-dimensional phonon interacting with two-dimensional exciton and include the deformation potential, the polar and the piezoelectric couplings. The expression for $C(k,k',q)$ is given in the next section. We can reexpress (3) in terms of polariton operator using the Hopfield transformation,[13]

$$H = \sum_{k,i=1,2,3}\Big\{E_i(k)(\alpha_{i,k}^\dagger \alpha_{i,k} + \tfrac{1}{2}) + E_a(k)(c_k^\dagger c_k + \tfrac{1}{2})\Big\} + \sum_{\substack{k,k',\\ i,j=1,2,3}} i\Xi_{i,j}(k,k')\alpha_{i,k'}^\dagger \alpha_{j,k}(c_{k'-k} - c_{k-k'}^\dagger), \tag{4}$$

where $\alpha_{i,k}$ is the polariton operator of branch i and wave vector k, and we keep only the terms in the Hamiltonian which describe the scattering of polariton with absorption and emission of phonon. We have

$$\Xi_{i,j}(k,k',q) = \begin{cases} C(k,k',q)(\varepsilon_\lambda \varepsilon'_{\lambda'})[u_j^*(k')u_i(k) + v_i^*(k)v_j(k')], & i,j = 1,2 \\ C(k,k',q)(\varepsilon_\lambda \varepsilon'_{\lambda'})u_i(k), & i = 1,2 \text{ and } j = 3 \\ C(k,k',q)(\varepsilon_\lambda \varepsilon'_{\lambda'})u_j^*(k'), & j = 1,2 \text{ and } i = 3 \\ C(k,k',q), & i,j = 3. \end{cases} \tag{5}$$

We denote the unit polarization vector ε, and the index $i = 1,2,3$ corresponds to the upper transverse, the lower transverse, and the longitudinal polariton branch, respectively. The longitudinal branch is not optically active but can be excited by scattering processes. For a transverse polariton, ε_λ has two orthonormal components, $\lambda = 1,2$, whereas for the longitudinal polariton, there is only one polarization component. The polarization factors, $(\varepsilon_\lambda \varepsilon'_{\lambda'})$, can be easily derived. From Fig. 1, we see that the final polarizations are given by $\varepsilon_1' = (\sin\varphi, -\cos\varphi, 0)$, $\varepsilon_2' = (\cos\theta\cos\varphi, \cos\theta\cos\varphi, -\sin\theta)$, $\varepsilon_3' = (\sin\theta\cos\varphi, \sin\theta\cos\varphi, \cos\theta)$. Thus, the polarization factor of scattering from transverse polariton to transverse polariton is $\sum_{\lambda,\lambda'=1,2}(\varepsilon_\lambda \varepsilon'_{\lambda'})^2 = 1 + \cos^2\theta$. Similarly the cases for transverse to longitudinal and longitudinal to longitudinal are given by $\sum_{\lambda=1,2}(\varepsilon_\lambda \varepsilon'_3)^2 = \sin^2\theta$ and $\sum_{\lambda,\lambda'=3}(\varepsilon_\lambda \varepsilon'_{\lambda'})^2 = \cos^2\theta$, respectively. We note that the Hamiltonian (4) has the form of coupled harmonic oscillator system with the polariton being the harmonic oscillator with a coupling constant dependent on the phonon population. The polariton dispersion and the coefficients $u_i(k)$ and $v_i(k)$ are given by

$$E_{1,2}(k) = \left[\frac{E_p(k)^2 + (1+g)E_{\rm ex}(k)^2 \pm \sqrt{[E_p(k)^2 + (1+g)E_{\rm ex}(k)^2]^2 - 4E_p(k)^2 E_{\rm ex}(k)^2}}{2}\right]^{1/2}, \tag{6}$$

$$E_3(k) = E_{\rm ex}(k)\sqrt{1+g},$$

$$u_i(k) = i\sqrt{\frac{g}{4E_i(k)E_{\rm ex}(k)g_i(k)}}\frac{E_{\rm ex}(k)+E_i(k)}{1-E_i(k)^2/E_{\rm ex}(k)^2},$$

$$v_i(k) = \frac{E_i(k)-E_{\rm ex}(k)}{E_i(k)+E_{\rm ex}(k)}u_i(k),$$

$$g_i(k) = 1+\frac{g}{[1-E_i(k)^2/E_{\rm ex}(k)^2]^2},$$

where we define the coupling constant $g \equiv 4\pi\beta/\varepsilon_\infty$. Here β is the quantum-well polarizability and ε_∞ is the high-frequency dielectric constant. The separation of energy between branch 1 and 2 at $k_\parallel = 0$ is $\Delta E = E_{\rm ex}(0)\sqrt{g}$ for $g \ll 1$. In general, the presence of damping makes it hard to relate the experimentally observed splitting to the coupling constant g since the observed peak maxima in this case do not correspond to E_1 and E_2. At very large damping the observed peaks "melt" into each other and one can only observe one peak although the two polariton branches still have different eigenenergies. The relation between g and ΔE will be the subject of a future paper. We note that (4) can be diagonalized exactly using a transformation similar to the Hopfield transformation; however, the resulting three dispersion branches are applicable only in the presence of an acoustic cavity.

A plot of the microcavity effective density of states for a one λ long GaAs/Al_xGa_{1-x}As dielectric microcavity is given in Fig. 2(a). The figure illustrates the S-polarized modes, but in the region of interest close to $k_\parallel = 0$, there is a negligible difference between the S-polarized and the P-polarized modes. The figure was calculated using the matrix method described in Ref. 14. It is seen that in addition to the cavity mode, with the dispersion essentially given by (2), there exist a mode continuum everywhere except in the stopband (the band where the Bragg mirrors are highly reflecting) surrounding the cavity mode. However, from Fig. 2(b), it is seen that for realistic values of the coupling constant the exciton and the photon mode couple only in a small region near $k_\parallel = 0$, corresponding to a propagation angle of less than 10° from the normal. It is also seen that the energy splitting is only a fraction of the cavity stopband width (15 meV vs 300 meV). Hence, the mode continuum contains energies so far removed from the excitonic resonance that it can be neglected. Therefore, it is permissible to use the highly idealized dispersion given by (2) when calculating the polariton dispersion.

III. PHONON SCATTERING RATES

In this section, the inelastic intravalley scattering rates for the microcavity polariton are derived. We consider only the $k_\parallel = 0$ polariton, the dressed exciton, assuming that the populations of $k_\parallel \neq 0$ polariton are small, and calculate the rate of scattering taking into account all three dispersion branches. Numerically, we find that the scattering rate for the lower branch is suppressed with increasing exciton-photon coupling, whereas the scattering rate for the upper branch stays roughly constant. The calculation can easily be extended to $k_\parallel \neq 0$ states. The wave vector of the phonon can be decomposed into two components, $q = (q_\parallel, q_z)$, with $q_\parallel$ (q_z) being parallel (perpendicular) to the quantum-well plane. For the confined polariton, the initial and final in-plane wave vectors are $k = k_\parallel$ and $k' = k'_\parallel$. Conservation of energy and momentum give

$$E_l(k_\parallel) - E_j(k'_\parallel) = \pm E_a(q), \tag{7}$$

$$q_\parallel^2 = k_\parallel^2 + k_\parallel'^2 - 2k_\parallel k'_\parallel\cos(\theta), \tag{8}$$

where θ is the angle between $k_\parallel$ and $k'_\parallel$, and the plus (minus) sign denotes absorption (emission) processes. Equations (7) and (8) greatly constrain the allowable final states of the polariton. For the purpose of calculating the exciton-phonon Hamiltonian, we use the exciton envelope wave function of the form[15]

$$f_{1s}(r,z_e,z_h) = \sqrt{\frac{8}{\pi}}\frac{\alpha}{L_z}\exp(-\alpha r)\cos\left(\frac{\pi z_h}{L_z}\right)\cos\left(\frac{\pi z_e}{L_z}\right), \tag{9}$$

where α is a variational parameter, $z_{e,h}$ are the electron and hole coordinates, and L_z the width of the quantum-well.

A. Acoustic phonon scattering

Depending on the initial or final polariton state, both phonon emission and absorption are possible. The phonon dispersion is approximated by $E_a(q) = \hbar u\sqrt{q_\parallel^2+q_z^2}$, where u is the acoustic velocity in the medium. Following a derivation similar to that of Takagahara[16] and using (9), the coupling for the deformation potential is given by

$$C_{\rm DF}(q_\parallel) = \sqrt{\frac{\hbar q_\parallel}{2\rho u V}}G(q_z)\left\{\frac{D_c}{[1+(b_h/2)^2]^{3/2}} - \frac{D_v}{[1+(b_e/2)^2]^{3/2}}\right\}, \tag{10}$$

where $D_{c,v}$ are the deformation potentials of the valence and conduction bands, V is the quantization volume of the phonon, ρ is the mass density of the semiconductor,

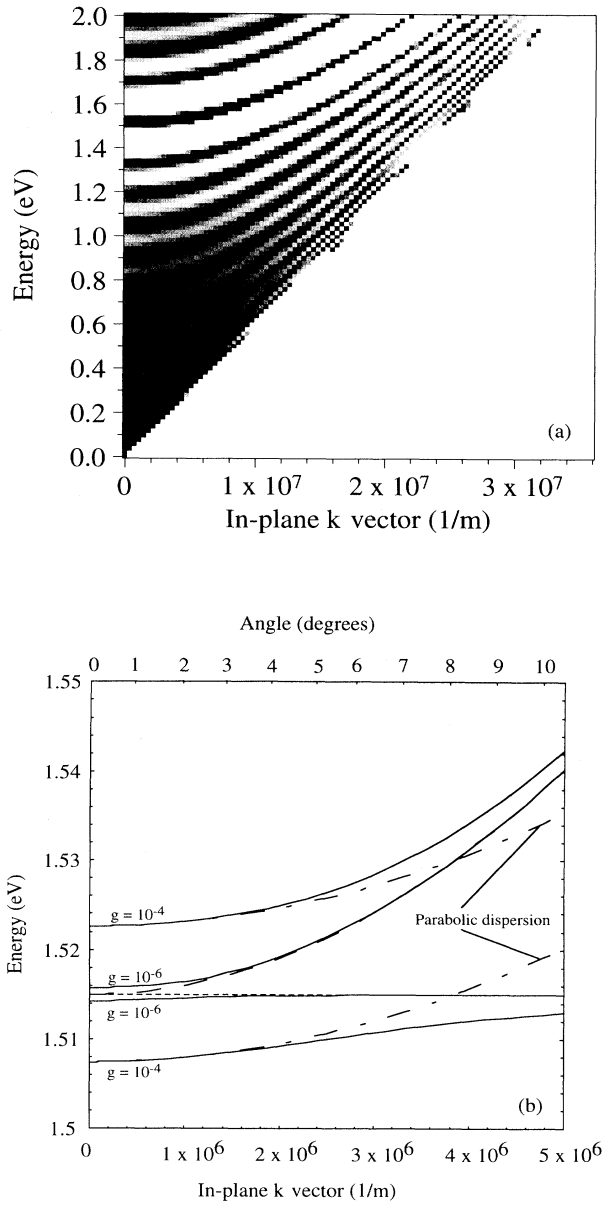

FIG. 2. (a) Raster image of the effective density of S-polarized states (TE modes) in a dielectric Bragg mirror microcavity with a one wavelength long "cavity" as a function of energy and $k_{\|}$. The resonant mode and its surrounding stopband (with a suppressed density of states) can clearly be seen extending out from $E \approx 1.51$ eV. The width of the mode appears much wider than it is in reality due to the finite raster resolution. On each side of the stopband, there is a weakly modulated continuum of modes. (b) Graph of the dispersion for an ideal planar microcavity for two different coupling constants g. The solid lines denote the coupled mode dispersion branches 1 and 2. The dotted lines denote uncoupled exciton dispersion and the dashed line the cavity-mode dispersion. The longitudinal exciton branch 3 coincides with the uncoupled exciton (dotted line) to within the resolution of the figure. The dash-dotted lines represent a parabolic dispersion. At the top of the graph the propagation angle inside the GaAs microcavity is shown.

$b_h = m_h q_{\|}/[(m_e+m_h)\alpha]$, $b_e = m_e q_{\|}/[(m_e+m_h)\alpha]$, $m_{e,h}$ are the electron and hole effective masses, and

$$G(q_z) = \frac{8\pi^2 \sin(q_z L_z/2)}{q_z L_z (4\pi^2 - q_z^2 L_z^2)}.$$

The piezoelectric coupling is highly anisotropic for the zinc blende. In order to simplify the problem, we take the spherical average of the piezoelectric constants for the longitudinal and the transverse mode,[17] and the coupling is simplified to

$$C_{\mathrm{PZ}}(q_{\|}) = \frac{eG(q_z)e_{14}}{\varepsilon_s \varepsilon_0}\sqrt{\frac{\hbar}{2\rho V q_{\|} u_{\mathrm{eff}}}}\left\{\frac{1}{[1+(b_h/2)^2]^{3/2}} - \tfrac{1}{2}\left[1+(b_e/2)^2\right]^{3/2}\right\}, \tag{11}$$

where we also neglect the energy differences between the longitudinal and the transverse phonon. In this equation e is the unit charge, ϵ_s is the relative static dielectric constant, e_{14} is the piezoelectric constant, and $u_{\mathrm{eff}} = [12/(35u_{\mathrm{LA}}) + 16/(35u_{\mathrm{TA}})]^{-1}$. To simplify the notation, we define $\gamma_{e(h)} = [1 + (b_{e(h)}/2)^2]^{-3/2}$ and $p_{i,f}(k) = [u_f^*(k)u_i(0) + v_i^*(0)v_f(k)](\varepsilon_i \varepsilon_f)$. The scattering rate for the deformation potential coupling with initial branch i and final branch f is given by

$$\begin{aligned} W_{\mathrm{DF},i,f} &= \frac{2\pi}{\hbar}\sum_f |p_{i,f}(k')C_{\mathrm{DF}}|^2 \delta[E_f(k') - E_i(0) \\ &\quad \pm \hbar u\sqrt{q_{\|}^2 + q_z^2}]n_q \\ &= \frac{\xi k_B T}{8\pi\rho u^2 \hbar} \\ &\quad \times \int_{-\infty}^{\infty} dq_z \frac{k'^2 (D_c\gamma_h - D_v\gamma_e)^2 G(q_z)^2 p_{i,f}(k')^2}{\left|\sqrt{k'^2+q_z^2}(dE_f/dk)_{k=k'} \pm \hbar u k'\right|}, \end{aligned} \tag{12}$$

where $q_{\|} = k'$, $\xi = 3$ (or 1) for intraband (or interband) scattering, $k'(q_z)$ is the root of $E_f(k') - E_i(0) = \pm\hbar u\sqrt{k'^2+q_z^2}$, and the plus (minus) sign denotes phonon absorption (emission). The rate for the particular process is zero if the root does not exist. For parameters of physical relevance, there exists only one root to the equation, but, in general, one must sum the rates for all the roots. For piezoelectric scattering, the rate is

$$\begin{aligned} W_{\mathrm{PZ},i,f} &= \frac{\xi e^2 e_{14}^2 k_B T}{8\pi\varepsilon_s^2\varepsilon_0^2\rho u_{\mathrm{eff}}^2\hbar} \\ &\quad \times \int_{-\infty}^{\infty} dq_z \frac{(\gamma_h - \gamma_e)^2 G(q_z)^2 p_{i,f}(k')^2}{\left|\sqrt{k'^2+q_z^2}(dE_f/dk)_{k=k'} \pm \hbar u k'\right|}. \end{aligned} \tag{13}$$

B. Optical phonon scattering

We consider the deformation potential and polar interactions in calculating the scattering rate of a polariton

by an optical phonon. In GaAs, the optical phonon energy is greater than the exciton binding energy, $E_a = 36$ meV $> E_{\rm bind} \simeq 8$ meV. In this calculation, we assume that the final polariton state consists of only a bound exciton state with extra kinetic energy and not of a free electron and hole state. This approximation gives an order of magnitude estimates of the scattering rates. The coupling for deformation potential is given by

$$C_{\rm DF}(q_\parallel) = \sqrt{\frac{\hbar}{2\rho\omega_a V}}(D_c'\gamma_h - D_v'\gamma_e)G(q_z), \tag{14}$$

with $D_{c,v}'$ replaced by the values appropriate for an optical phonon.[17] Assuming the dispersion of the optical phonon to be independent of wave vector, $E_a(q) = \hbar\omega_a$, the scattering rate is given by

$$\begin{aligned} W_{{\rm DF},i,f} &= \frac{\xi n_q}{8\pi\rho\omega_a}\int_{-\infty}^{\infty} k'dq_z\,(D_c'\gamma_h - D_v'\gamma_e)^2 \\ &\quad\times G(q_z)^2 p_{i,f}(k')^2\left(\frac{dE_f}{dk}\right)^{-1}_{k=k'} \\ &= \frac{3\xi n_q k'}{8\rho\omega_a L_z}(D_c'\gamma_h - D_v'\gamma_e)^2 p_{i,f}(k')^2\left(\frac{dE_f}{dk}\right)^{-1}_{k=k'}, \end{aligned} \tag{15}$$

with $q_\parallel = k'$ and k' being the root of $E_f(k') - E_i(0) \pm \hbar\omega_a = 0$. The relaxation time approximation is not valid for the case of polar optical phonon scattering because the scattering is neither elastic nor randomizing;[18] nonetheless, we assume that a rate exists and use the interaction of the form

$$C_{\rm PO}(q_\parallel) = \frac{e}{q_\parallel}\sqrt{\frac{\hbar\omega_a}{2\varepsilon_p\varepsilon_0 V}}(\gamma_h - \gamma_e)G(q_z), \tag{16}$$

with $\varepsilon_p^{-1} = \varepsilon_\infty^{-1} - \varepsilon_s^{-1}$. The scattering rate for this case is given by

$$\begin{aligned} W_{{\rm PO},i,f} &= \frac{\xi e^2\omega_a n_q}{8\pi\varepsilon_p\varepsilon_0}\int_{-\infty}^{\infty}\frac{dq_z}{k'}\,(\gamma_h - \gamma_e)^2 \\ &\quad\times G(q_z)^2 p_{i,f}(k')^2\left(\frac{dE_f}{dk}\right)^{-1}_{k=k'} \\ &= \frac{3\xi e^2\omega_a n_q}{8\varepsilon_p\varepsilon_0 k' L_z}(\gamma_h - \gamma_e)^2 p_{i,f}(k')^2\left(\frac{dE_f}{dk}\right)^{-1}_{k=k'}. \end{aligned} \tag{17}$$

C. Comparison of bare and dressed exciton scattering rates

Combining all the results in the previous sections, we can calculate the total scattering rate of the $k_\parallel = 0$ polariton (the dressed exciton) including intraband and interband scatterings. For the numerical computation, we use the parameters $a_B = 13.6$ nm, $\alpha = 1.1a_B^{-1}$,[15] $L_z = 20$ nm, $M = m_h + m_e$, $E_{1s} = 1.515$ eV, $u_{\rm LA} = 4.81\times10^3$ m/s, $u_{\rm TA} = 3.34\times10^3$ m/s, $\rho = 5.307\times10^3$ kg/m^3, $D_v = 12.0$ eV, $D_c = -6.1$ eV, $e_{14} = 0.16$ C/m^2, $\varepsilon_\infty = 10.9$, $\varepsilon_s = 12.8$, $m_e = 0.067m_0$, $m_h = 0.45m_0$, $\hbar\omega_a = 36.2$ meV, $D_c' = -2\times10^{11}$ eV/m, and $D_v' = 2\times10^{11}$ eV/m. The parameter, $g = 4\pi\beta/\varepsilon_\infty$ measures the magnitude of the photon-exciton coupling. When $g = 0$, (6) reduces to the bare exciton and bare photon dispersion. Depending on the coupling factor, g, we find the total scattering rate to be

$$W_{\rm tot} = \alpha_1(g)T + \frac{\alpha_2(g)}{e^{E_a/k_BT} - 1}. \tag{18}$$

Variation of $\alpha_{1,2}$ with g is shown in Fig. 3, and a plot of the rates for different g is given in Fig. 4 for the lower and upper polariton branches. These rates can be compared with that of the bare exciton,[19] and we find that, in general, the scattering rate for the dressed exciton in the lower branch by phonons is smaller. In particular, the acoustic phonon scattering at low temperature is suppressed. To understand the origin of the suppression, we look at the curvature or effective mass of the polariton. We note that, in two dimensions, the density of state for the parabolic band is linearly proportional to the effective mass. The polariton dispersion near $k_\parallel = 0$ is approximately parabolic in the upper branch with an effective mass given by

$$m_{\rm eff} = \frac{2m_{\rm ex}m_p}{m_{\rm ex} + m_p} \simeq 2m_p, \tag{19}$$

where $m_p = E_{1s}n^2/c^2$ can be interpreted as the cavity photon effective mass. The naive interpretation of this equation is that the polariton is a photon (with small mass) half of the time and an exciton (with large mass) the other half of the time. Any "force" on the polariton will move the polariton with an acceleration proportional to the inverse of the effective mass. Essentially the movement is restricted to the time when the exciton is light (no pun intended) and the acceleration during that time will be determined by the photon mass. Therefore, one expects the effective mass of the polariton to be given by

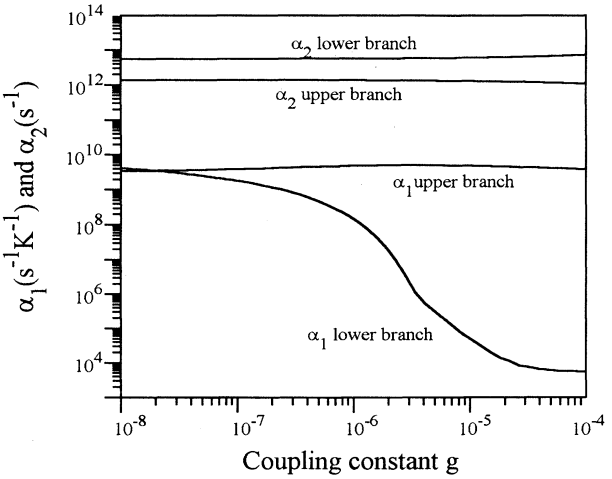

FIG. 3. Graph of the scattering rate coefficients α_1 and α_2 vs the coupling constant g, for the optically active upper and lower branches.

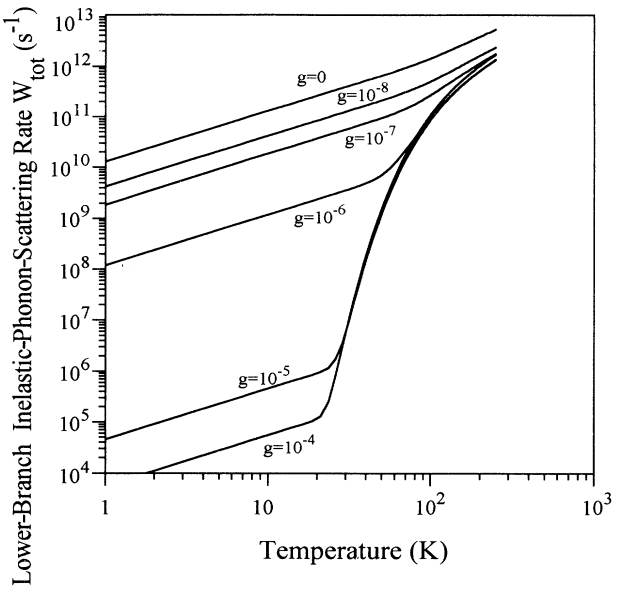

FIG. 4. Graph of the lower branch polariton scattering rate $W_{\rm tot}(T)$ as a function of temperature for different coupling $g = 0$ (uncoupled exciton), 10^{-8}, 10^{-7}, 10^{-6}, 10^{-5}, 10^{-4}.

twice the photon mass in agreement with (19). For larger $k_{||}$ the effective mass of the upper polariton branch goes monotonically to the photon mass, as expected.

For both the upper and lower branches, we can actually divide the dispersion into three regions (Fig. 5), although the distinction between the regions is clearer for the lower branch. For small $k_{||}$, region 1, the dispersion for both branches is parabolic with the mass given by (19). This is the region where it is actually appropriate to talk about a cavity polariton, or a cavity dressed exciton. In this region, both branches are identical, except for their eigenenergies. Although the

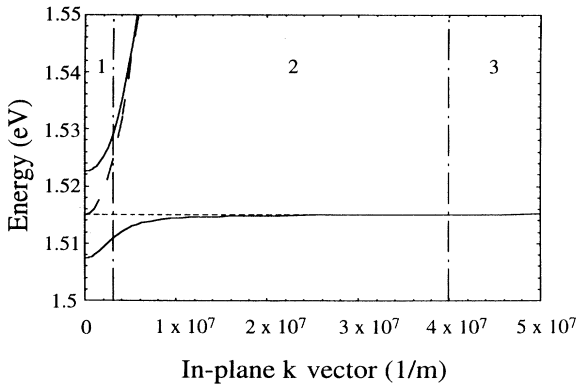

FIG. 5. The three dispersion branches at resonance for $g = 10^{-4}$. The dotted and dashed lines represent the dispersion curves of the uncoupled exciton and photon, respectively. The numbers 1, 2, and 3 separated by dash-dotted vertical lines indicate the three dispersion regions. The curvature of the lower branch in region 3 can hardly be seen in the figure due to the comparatively large exciton mass.

cavity polaritons in both branches are mathematically in an equal superposition of a photon and an exciton, physically both branches are more photonlike than excitonlike. For any $k_{||}$ within the region, the energy splitting between the branches is constant. In Fig. 2(b) an expanded view of this region can be seen, including, for illustration purposes, two dash-dotted displaced parabolic dispersion curves with an effective mass equal to (19). For large $k_{||}$, the dispersion is parabolic (with mass given by $m_{\rm ex}$) for the lower branch and cavity-mode-like for the upper branch. In this third region it is not really appropriate to talk about cavity polaritons anymore, because the coupling between the exciton and the cavity mode is negligible. In region 2, between 1 and 3, the dispersion of the lower branch depends strongly on the coupling g and is nonparabolic. The size of the first parabolic region, Δk, is only weakly dependent on coupling, and for the given parameters it varies as $\Delta k \approx 3 \times 10^7 g^{1/4}$ m^{-1}. The region where the two branches are almost uncoupled is given by $k_{||} > 4 \times 10^8 g^{1/4}$ m^{-1}. In the limit of $g \to 0$, this means that the dispersion curves becomes uncoupled with exciton and photon character, respectably. Note, however, that for a nonzero coupling, irrespective of the coupling strength, there always exist a region near $k_{||} = 0$, where the dispersion of the two branches are similar and have effective masses according to (19).

In view of the above, the suppression of scattering rate can be seen to be caused by the presence of the first region. Physically, the coupling of the exciton with a microcavity photon mode drastically modifies the exciton dispersion within a range of Δk. The increased curvature of the dispersion, or equivalently the reduction of the effective mass, decreases the density of final scattered state and the intraband scattering rate for the lower branch. Note that this decrease is substantial since $M \approx 5 \times 10^{-31}$ kg, whereas $m_{\rm eff} \approx 7 \times 10^{-35}$ kg. The relations (7) and (8) restrict the type of final states that the $k_{||} = 0$ polariton can couple to, leading to a decrease of dressed exciton scattering rate as long as $kT < (E_1 - E_2)/2$. This last relation is derived noting that this is the energy required to scatter a polariton from $k_{||} \approx 0$ to the region where the dispersion of the lower branch is excitonlike. We find numerically that for an initial state $k_{||} = 0$ at the lower branch, the main contributions to the scattering rate are intraband scattering and interband scattering to the final state at the longitudinal exciton branch $E_3(k)$ as defined in (6). The scattering to the upper branch is negligible. For the case where the initial state is the $k_{||} = 0$ polariton at the upper branch. The dominant contributions come from interband scattering where the final states are at the longitudinal exciton branch and the lower branch.

IV. RATE EQUATION MODEL

A. Heisenberg equation of motion

In this section, we derive a rate equation that describes the polariton dynamics inside a microcavity. The starting point is the Hamiltonian (4) with couplings to reservoirs. In a real experiment, the microcavity is not a closed system and is subject to dissipation, which can be modeled

by coupling of the microcavity photon field to a photon bath, or equivalently, the microcavity polariton field to a polariton bath. Coupling to a bath introduces well known damping and fluctuation terms under the Markoff approximation.[7] If we include the presence of the polariton bath, the Heisenberg equations of motion for the amplitude of the polariton and phonon fields are

$$\frac{d\alpha_{l,k}}{dt} = -\frac{iE_l(k)}{\hbar}\alpha_{l,k} - \gamma_{l,k}\alpha_{l,k} + \sum_{k',j}\frac{\Xi_{l,j}(k',k,q)}{\hbar}\alpha_{j,k'}(c_{k-k'} - c^\dagger_{k'-k}) + F_{l,k}(t), \tag{20}$$

$$\frac{dc_q}{dt} = \frac{-iE_a(q)}{\hbar}c_q - \sum_{k',i,j}\frac{\Xi_{i,j}(k',k'-q,q)}{\hbar}\alpha^\dagger_{i,k'-q}\alpha_{j,k'}, \tag{21}$$

where $\gamma_{l,k}$ is the net amplitude damping for polariton in branch l and of wave vector k, and $F_{l,k}(t)$ is the net fluctuation operator due to the polariton bath. Since we are not interested in the noise properties of our system, we neglect $F_{l,k}(t)$ from now on. We define the number operators $N_{l,k} \equiv \alpha^\dagger_{l,k}\alpha_{l,k}$ and $n_q \equiv c^\dagger_q c_q$. Using $dN/dt = \alpha^\dagger\,\dot{\alpha} + \dot{\alpha}^\dagger\,\alpha$, we can derive the equations for the occupation number,

$$\left(2\gamma_{l,k} + \frac{d}{dt}\right)N_{l,k} = \sum_{k',j}\frac{\Xi_{l,j}(k',k,q)}{\hbar}\alpha^\dagger_{l,k}\alpha_{j,k'} \times (c_{k-k'} - c^\dagger_{k'-k}) + \text{H.c.}, \tag{22}$$

$$\frac{dn_q}{dt} = -\sum_{k',i,j}\frac{\Xi_{i,j}(k',k'-q,q)}{\hbar}\alpha^\dagger_{i,k'-q}\alpha_{j,k'}c^\dagger_q + \text{H.c.} \tag{23}$$

Having obtained the rate equations, we make the adiabatic approximation[6] on the transition operators $\alpha^\dagger_{l,q}\alpha_{j,k'}c_{q-k'}$ and $\alpha^\dagger_{l,q}\alpha_{j,k'}c^\dagger_{k'-q}$ next. For example, we set

$$\frac{d\alpha^\dagger_{l,k}\alpha_{j,k'}c_{k-k'}}{dt} = \left[i\frac{E_l(k) - E_j(k') - E_a(k-k')}{\hbar} - (\gamma_{l,k} + \gamma_{j,k'})\right]\alpha^\dagger_{l,k}\alpha_{j,k'}c_{k-k'} + \frac{\Xi_{j,l}(k,k',q)}{\hbar}[(N_{j,k'} - N_{l,k})n_{k-k'} - N_{l,k}(N_{j,k'}+1)] = 0$$

and substitute the steady state values for the transition operators into (22) to get

$$\left(2\gamma_{l,k} + \frac{d}{dt}\right)N_{l,k} = \sum_{k',j}2(\gamma_{l,k} + \gamma_{j,k'})\,|\Xi_{l,j}(k',k,q)|^2 \times \left\{\frac{(N_{j,k'} - N_{l,k})(n_{k-k'}+1) - N_{j,k'}(N_{l,k}+1)}{[E_l(k) - E_j(k') - E_a(k-k')]^2 + \hbar^2(\gamma_{l,k} + \gamma_{j,k'})^2} + \frac{(N_{j,k'} - N_{l,k})n_{k'-k} + N_{j,k'}(N_{l,k}+1)}{[E_l(k) - E_j(k') + E_a(k-k')]^2 + \hbar^2(\gamma_{l,k} + \gamma_{j,k'})^2}\right\}. \tag{24}$$

Note that from now on, we treat $N_{l,k}$ as expectation value and not as operator. Using the identity,

$$\delta(x) = \lim_{a\to 0}\frac{1}{\pi}\frac{a}{x^2 + a^2},$$

and setting $(\gamma_{l,k} + \gamma_{j,k'}) = 0$, we arrive at the final result,

$$\left(2\gamma_{l,k} + \frac{d}{dt}\right)N_{l,k} = P_{l,k}(t) + \frac{2\pi}{\hbar}\sum_{k',j}|\Xi_{l,j}(k',k,q)|^2 \times\{[N_{j,k'}n_{k-k'}(N_{l,k}+1) - N_{l,k}(n_{k-k'}+1)(N_{j,k'}+1)]\delta[E_l(k) - E_j(k') - E_a(k-k')] + [N_{j,k'}(n_{k'-k}+1)(N_{l,k}+1) - N_{l,k}n_{k'-k}(N_{j,k'}+1)]\delta[E_l(k) - E_j(k') + E_a(k-k')]\}. \tag{25}$$

We have also added a phenomenological pump term $P_{l,k}(t)$. In setting $(\gamma_{l,k} + \gamma_{j,k'}) = 0$, we assume that the polariton damping rate γ is long in comparison with scattering process. This is especially true for longitudinal excitons and excitons with a large wave vector which are optically inactive. To simplify the calculation, we consider the phonon fields as a classical reservoir and set $n_q = 1/(e^{\beta E_a(q)} - 1) \simeq k_B T/E_a(q)$, i.e., the Bose-Einstein distribution. In making the above simplification, we assume that the phonon field is always in thermal equilibrium, i.e., the thermalization time of a phonon is very fast, and that energy normalization, energy damping and any type of fluctuation by phonon are negligible. For the case where the damping of the polariton is dominated by leakage of photons from the microcavity, we can set

$$\gamma_{l,k} = \gamma(k_\parallel)\left[\frac{E_p(k_\parallel)^2 + E_l(k_\parallel)^2}{2E_p(k_\parallel)E_l(k_\parallel)g_l(k_\parallel)}\right],$$

where $\gamma(k_\parallel)$ is the microcavity photon loss rate which can be calculated from a transfer matrix formalism,[14] $l = 1, 2$ and the coefficient following $\gamma(k_\parallel)$ measures the photon component of the polariton. We solve (25) numerically by considering all three dispersion branches. Figure 6 shows the typical behavior of the polariton steady state distribution for the lowest branch. The pump is set at finite $k_\parallel$ or finite angle $\psi = \tan^{-1}(k_\parallel L_z/2\pi)$. At low pump intensity, the majority of the polaritons are centered at the pump wave vector. As the pump increases, the polariton population is scattered to the $k_\parallel = 0$ state due to its coupling to the phonon bath. The net result is a buildup of polariton population at $k_\parallel = 0$, which is analogous to the bottleneck effect of the bulk polariton.

To simplify (25), which is a nonlinear integro-differential equation of a distribution function, we divide the polaritons into two populations, the dressed exciton population in region 1 with $k \simeq 0$ and mean occupation number N_1, and propagating polariton modes with $k \neq 0$ in region 2 and 3 and higher branches and mean occupation number N_{2i}. We consider the following scattering processes shown in Fig. 7:

$$\text{POLARITON}_{k\neq 0} \Longleftrightarrow \text{POLARITON}_{k_\parallel=0} + \text{PHONON},$$

with a coupling constant of C. Since we treat the $k_\parallel = 0$ population to be at the lowest energy state, we can ignore the process,

$$\text{POLARITON}_{k_\parallel=0} \Longleftrightarrow \text{POLARITON}_{k\neq 0} + \text{PHONON}.$$

The rate equations for the simple scattering process are

$$\frac{dN_1}{dt} = P - \frac{N_1}{\tau_1} - \sum_i C_i\left[N_1 n - N_{2i}(n+1)(N_1+1)\right], \tag{26}$$

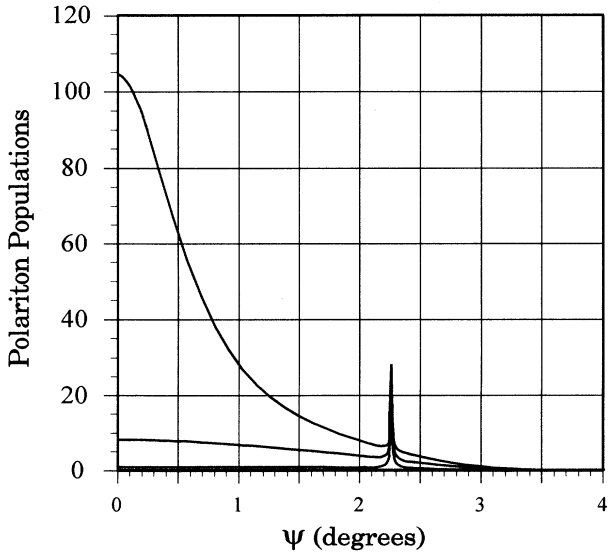

FIG. 6. Steady state polariton distribution for the lower branch with $P_{l,k}(t) = P_0\delta(k - 10^6\ \text{m}^{-1})$ for different values of P_0.

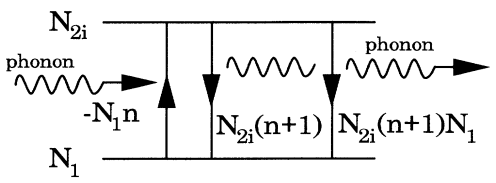

FIG. 7. Level diagram of polariton transitions.

$$\frac{dN_{2i}}{dt} = -\frac{N_{2i}}{\tau_{2i}} + C_i\left[N_1 n - N_{2i}(n+1)(N_1+1)\right], \tag{27}$$

where the sum is taken over all modes i, τ_1, and τ_{2i} are mean lifetimes for polaritons, and we neglect scattering between $k_\parallel \neq 0$ modes. We also neglect stimulated emission of $k \neq 0$ polariton by setting $nN_1(N_{2i}+1) \simeq nN_1$. The population of $k \neq 0$ polariton is presumably low since the stimulated absorption process that populates this polariton requires feedback which is only available to k near zero polariton. Equations (26) and (27) can be considered as a simple discretized version of (25). For simplicity, we again treat the phonon system as a reservoir. Inclusion of phonon equation of motion will lead to hysteresis behavior in the polariton population. The lifetimes τ_1 and τ_{2i} are mainly caused by the cavity leakage and, in general, $\tau_{2i} > \tau_1$. In solving (26) and (27), we make the assumption that τ_{2i}, C_i and n to be independent of index i. With this assumption, we define an effective polariton population $N_2 = \sum_i N_{2i}$ and an effective mode number, M, in which i goes from 1 to M. At steady state, all time derivatives are zero, and the equilibrium populations are given by

$$N_1 = \frac{-b - \sqrt{b^2 - 4ac}}{2a}, \tag{28}$$

$$N_{2i} = \frac{N_2}{M} = \frac{W_{\text{tot}}(T)N_1}{[M\tau_2^{-1} + W_{\text{tot}}(T)] + W_{\text{tot}}(T)N_1}, \tag{29}$$

$$a = -\frac{W_{\text{tot}}(T)}{\tau_1},$$

$$b = PW_{\text{tot}}(T) - \frac{M}{\tau_1\tau_2}[1 + M^{-1}\tau_2 W_{\text{tot}}(T) + \tau_1 W_{\text{tot}}(T)],$$

$$c = \frac{PM}{\tau_1\tau_2}[\tau_1 + W_{\text{tot}}(T)\tau_1 M^{-1}\tau_2],$$

where we set $CMn \simeq CM(n+1) \simeq W_{\text{tot}}(T)$. We can define a threshold for the above stimulated emission in which the population of N_{2i} is clamped at half the quasi-equilibrium value, i.e., $N_{2i} = 1/2$.[20] From (29), this threshold occurs when

$$N_{1\text{th}} = \frac{M\tau_2^{-1} + W_{\text{tot}}(T)}{W_{\text{tot}}(T)} \tag{30}$$

so that $N_{1\text{th}}$ is a strong function of temperature. There are three processes which are depleting the population of the $k \neq 0$ polariton: (1) leakage rate $M\tau_2^{-1}$, (2) spontaneous emission rate to $k = 0$, $W_{\text{tot}}(T)$, and (3) stimulated emission rate to $k = 0$, $W_{\text{tot}}(T)N_1$. The physical meaning of (30) is that the threshold occurs when the

population N_{2i} is clamped, at which point the sum of the rates (1) and (2) equals to the rate of (3). We treat the product, $M\tau_2^{-1}$, as a fitting parameter and set τ_1 to be half the photon decay rate. Figure 8 shows a plot of N_1 for different temperatures and input pump intensities. We defined the quantum efficiency as $\tau_1^{-1}N_1/P$ and the differential quantum efficiency as $\tau_1^{-1}dN_1/dP$. The results are interpreted as follows. At low temperature, the phonon population is low, and there is negligible phonon scattering. The dressed exciton population N_1 varies linearly with the coherent pump rate. In this case, the differential quantum efficiency is close to unity, and the polariton population N_{2i} is negligible. At high temperature, scattering by phonons is important, and the differential quantum efficiency is smaller than one due to the buildup of the polariton population. The dressed exciton population builds up only when the stimulated emission rate becomes appreciable. At this point, polaritons are converted to dressed exciton, and N_{2i} is clamped below unity. This parametric process is inherently different from the normal lasing process and exhibits a different threshold behavior. In the normal lasing process, the threshold occurs at $N_1 = 1$ independent of temperature. For the parametric process, the threshold is given by (30).

B. Comparison of model and experimental result

The experimental results taken from Ref. 1 are reproduced in Fig. 9 for comparison. The data are taken from a metal organic chemical vapor deposition grown sample with a single quantum-well embedded inside a microcavity.[8] The normal mode splitting is observed to be 0.15 nm (0.3 meV), and the oscillating period of the emission is measured to be 14 ps.[3] The observed coherent oscillating emission for a duration of 50 ps suggests

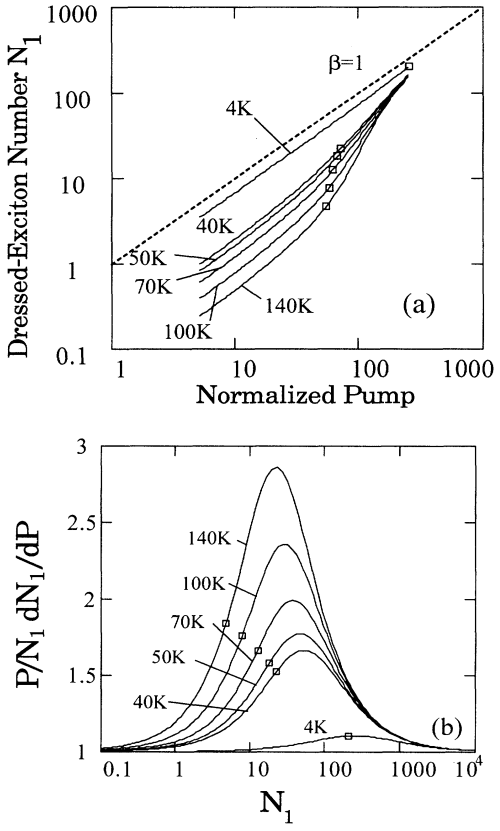

FIG. 8. (a) The steady state values of polariton population, N_1, at different temperatures. Squares denote the location of the threshold as defined in (30). The parameters are $\tau_1 = \tau_{2i} = 50$ ps, $M = 20$, and $g = 10^{-7}$. The dimensionless normalized pump is defined as $P\tau_1$. (b) Plot of the normalized differential quantum efficiency $P/N_1\ dN_1/dP$ vs N_1.

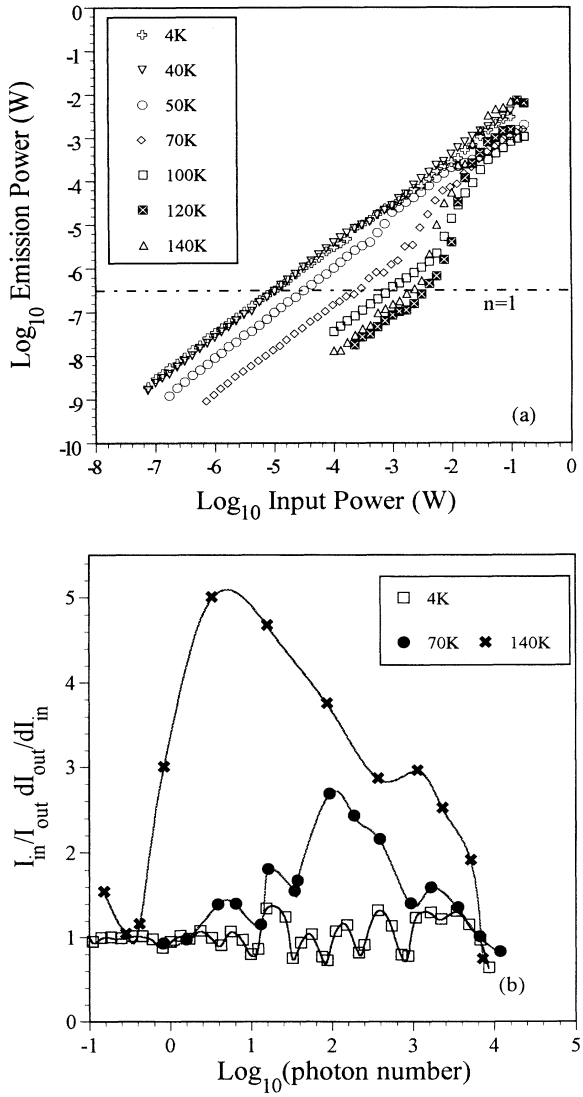

FIG. 9. (a) Planar microcavity input/output characteristics for different temperatures under cw resonant excitation. (b) $I_{\mathrm{in}}/I_{\mathrm{out}}\ dI_{\mathrm{out}}/dI_{\mathrm{in}}$ vs photon number n under cw resonant excitation.

that the dressed exciton dephasing time is fairly long at 4.2 K. The input-output characteristics of the microcavity are shown in Fig. 9(a). At 4 K, the differential quantum efficiency is independent of pump rate and is equal to one ($\beta = 1$, thresholdless behavior). With increasing temperature above 40 K, the differential quantum efficiency decreases at low pump rates. However, if the pump rate exceeds a certain threshold value, the differential quantum efficiency increases and eventually it becomes unity. This threshold behavior is very different from a conventional laser threshold. A conventional laser threshold occurs when the photon number of a lasing mode reaches unity,[8] and the emission below the threshold is incoherent spontaneous emission. The threshold shown in Fig. 9(a) occurs at the internal photon number much greater than one. This is clearly seen in Fig. 9(b), where the normalized differential quantum efficiency, $PN_1^{-1}dN_1/dP$, is plotted. The internal photon number at which the threshold is observed monotonically increases with the temperature. The temperature dependency of the threshold is a signature of parametric process between the dressed exciton and the phonon.

V. DISCUSSION

In this last section, we wish to discuss the approximations we made in the model and summarize our results. In our model, we have explicitly neglected the trapping of excitons by defects and the scattering of excitons by well width fluctuations, alloys, and impurities. These scattering processes are elastic and do not change the exciton energy distribution. On the other hand, trapping localizes the exciton, changing the exciton wave functions and the radiative decay rate. Since we consider the dressed exciton to be at $k_{||} = 0$, these excitons which are spatially stationary are unlikely to be scattered or trapped. A more subtle issue is the use of the microcavity exciton-polariton in our model. The description of the coupled exciton and photon modes as polariton modes are certainly valid when both the exciton and photon wave vectors are near zero, $k_{||} \simeq 0$. The observation of normal mode splitting supports this picture.[2,3] However, for large transverse wave vectors, the microcavity becomes leaky. The exciton is no longer strongly coupled to the microcavity photon mode, and the polariton picture breaks down. In a perfect bulk crystal, the polariton modes are temporally stationary. In a microcavity, the polariton modes with large wave vector are not even temporally quasistationary and are highly damped. Nonetheless, we are interested only in the dynamics of the polaritons with a wave vector close to zero so that polaritons with large wave vectors have a low occupation. As such, we believe that the microcavity polariton model gives the correct picture of the exciton-photon dynamics inside the microcavity. We also note that the dispersion given by (6) is for a single exciton, and any inhomogeneity will tend to "smear" the dispersion curves.

To conclude, we have shown that the interaction of polariton with phonon can lead to a temperature dependent threshold behavior. This stimulated emission of dressed exciton is observed in Ref. 1. In calculating the inelastic scattering rate of the dressed exciton by phonon for the case where $E_p(0) = E_{ex}(0)$, we find that the scattering rates by acoustic phonon are suppressed for the lower branch. The origin of the suppression is shown to be the reduction of polariton effective mass near $k_{||} = 0$. This effect becomes small when the exciton is detuned from the cavity photon mode.

ACKNOWLEDGMENTS

S.P. wishes to acknowledge financial support from the John and Fannie Hertz Foundation and would like to thank Dr. T. Takagahara of NTT Basic Research Laboratory, Dr. Johnson Lee of GTE Lab, Professor E. Hanamura of Tokyo University, and Professor W. A. Harrison of Stanford University for many helpful discussions. The authors also thank Dr. F. Matinaga of NTT Basic Research Laboratory for supplying experimental data for Fig. 9 and Dr. L. C. Andreani at Università di Pavia for sending us copies of his unpublished work.

* Also with NTT Basic Research Laboratories, Atsugishi, Kanagawa, Japan.

[1] Y. Yamamoto, F. Matinaga, S. Machida, A. Karlsson, J. Jacobson, G. Björk, and T. Mukai, J. Phys. (France) II **3**, 39 (1993).
[2] C. Weisbuch, M. Nishioka, A. Ishikawa, and Y. Arakawa, Phys. Rev. Lett. **69**, 3314 (1992).
[3] J. Jacobson, S. Pau, H. Cao, G. Björk, and Y. Yamamoto, Phys. Rev. A (to be published).
[4] H. Haug, J. Appl. Phys. **39**, 4687 (1968).
[5] E. Hanamura and H. Haug, Phys. Rep. **33**, 209 (1977).
[6] H. Haug and S. Koch, Phys. Status Solidi B **82**, 531 (1977).
[7] W. H. Louisell, *Quantum Statistical Properties of Radiation* (Wiley, New York, 1973).
[8] G. Björk, H. Heitmann, and Y. Yamamoto, Phys. Rev. A **47**, 4451 (1993).
[9] L. C. Andreani, in *Confined Electrons and Photons: New Physics and Devices*, edited by E. Burstein and C. Weisbuch (Plenum Press, New York, 1994).
[10] M. V. Klein, IEEE J. Quantum Electron. **QE-22**, 1760 (1986).
[11] W. C. Tait and R. L. Weiher, Phys. Rev. **178**, 1404 (1969).
[12] A. Quattropani, L. C. Andreani, and F. Bassani, Nuovo Cimento D **7**, 55 (1986).
[13] J. J. Hopfield, Phys. Rev. **112**, 1555 (1958).
[14] G. Björk, Y. Yamamoto, S. Machida, and K. Igeta, Phys. Rev. A **44**, 669 (1991).
[15] Y. Shinozuka and M. Matsuura, Phys. Rev. B **29**, 3717 (1984).
[16] T. Takagahara, Phys. Rev. B **31**, 6552 (1985).
[17] B. K. Ridley, *Quantum Processes in Semiconductors* (Oxford University Press, Oxford, 1993).

[18] B. R. Nag, *Theory of Electrical Transport in Semiconductors* (Pergamon Press, New York, 1972).
[19] J. Lee, E. S. Koteles, and M. O. Vassell, Phys. Rev. B **33**, 5512 (1986).
[20] If the stimulated emission term is taken into account, then there is a possibility of population buildup for the $k \neq 0$ polariton. In this case, the natural definition of lasing threshold is the point where $N_{2i} = n$, i.e., when the $k \neq 0$ polariton has the same population as the population of the phonon bath.

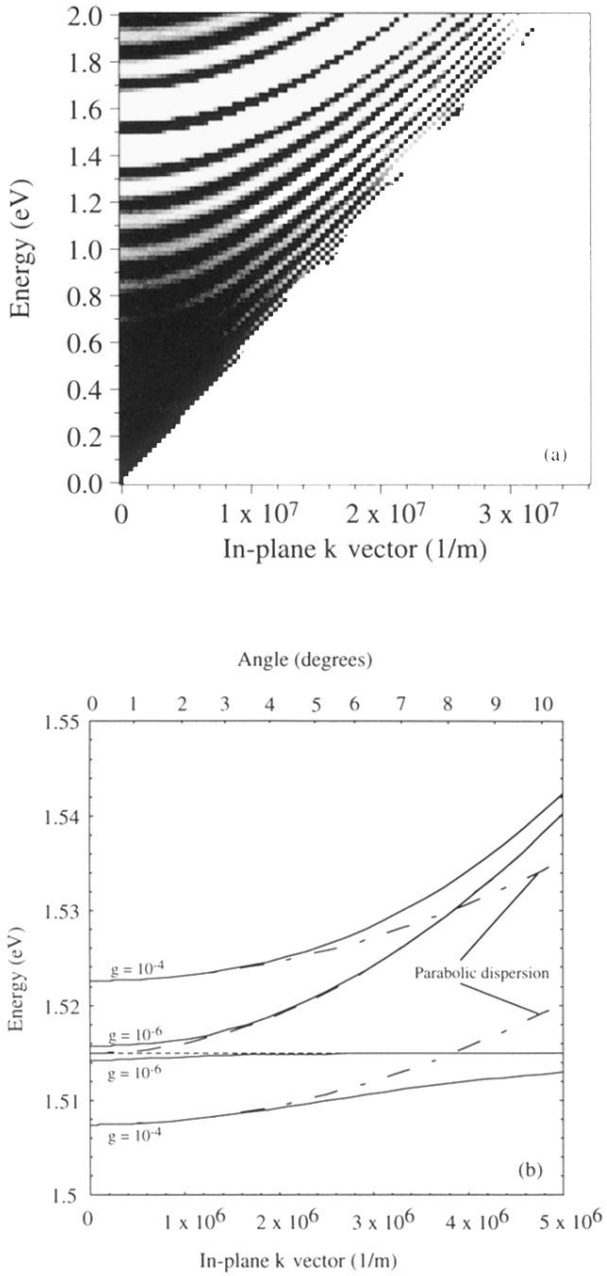

FIG. 2. (a) Raster image of the effective density of S-polarized states (TE modes) in a dielectric Bragg mirror microcavity with a one wavelength long "cavity" as a function of energy and $k_{\|}$. The resonant mode and its surrounding stopband (with a suppressed density of states) can clearly be seen extending out from $E \approx 1.51$ eV. The width of the mode appears much wider than it is in reality due to the finite raster resolution. On each side of the stopband, there is a weakly modulated continuum of modes. (b) Graph of the dispersion for an ideal planar microcavity for two different coupling constants g. The solid lines denote the coupled mode dispersion branches 1 and 2. The dotted lines denote uncoupled exciton dispersion and the dashed line the cavity-mode dispersion. The longitudinal exciton branch 3 coincides with the uncoupled exciton (dotted line) to within the resolution of the figure. The dash-dotted lines represent a parabolic dispersion. At the top of the graph the propagation angle inside the GaAs microcavity is shown.